Check for updates

View Article Online
View Journal

NJC

Accepted Manuscript

This article can be cited before page numbers have been issued, to do this please use: V. M. M. Nurchi, M. D. G. Jaraquemada-Pelaez, J. I. I. Lachowicz, M. A. Zoroddu, M. F. Peana, A. Dominguez-Martin, D. Choquesillo-Lazarte, M. Remelli, Z. Szewczuk and G. Crisponi, *New J. Chem.*, 2018, DOI: 10.1039/C7NJ03947F.

Volume 40 | Number 1 | January 2016 | Pages 1–846

NJC

New Journal of Chemistry
www.rsc.org/njc

A journal for new directions in chemistry

ISSN 1144-0546

ROYAL SOCIETY OF CHEMISTRY

PAPER
Jason B. Benedict et al.
The role of atropisomers on the photo-reactivity and fatigue of diarylethene-based metal–organic frameworks

This is an Accepted Manuscript, which has been through the Royal Society of Chemistry peer review process and has been accepted for publication.

Accepted Manuscripts are published online shortly after acceptance, before technical editing, formatting and proof reading. Using this free service, authors can make their results available to the community, in citable form, before we publish the edited article. We will replace this Accepted Manuscript with the edited and formatted Advance Article as soon as it is available.

You can find more information about Accepted Manuscripts in the author guidelines.

Please note that technical editing may introduce minor changes to the text and/or graphics, which may alter content. The journal's standard Terms & Conditions and the ethical guidelines, outlined in our author and reviewer resource centre, still apply. In no event shall the Royal Society of Chemistry be held responsible for any errors or omissions in this Accepted Manuscript or any consequences arising from the use of any information it contains.

ROYAL SOCIETY OF CHEMISTRY

rsc.li/njc

View Article Online
DOI: 10.1039/C7NJ03947F

Looking at new ligands for chelation therapy

Valeria Marina Nurchi[a*], Maria de Guadalupe Jaraquemada-Pelaez[b], Joanna I. Lachowicz[a], Maria Antonietta Zoroddu[c], Massimiliano Peana[c], Alicia Domínguez-Martín[d], Duane Choquesillo-Lazarte[e], Maurizio Remelli[f], Zbigniew Szewczuk[g], Guido Crisponi[a],

[a] Dipartimento di Scienze Chimiche e Geologiche, Università di Cagliari, Cittadella Universitaria, I-09042 Monserrato-Cagliari, Italy
[b] Medicinal Inorganic Chemistry Group, Department of Chemistry, University of British Columbia, 2036 Main Mall, Vancouver, BC, Canada
[c] Dipartimento di Chimica e Farmacia, Università di Sassari, Via Vienna 2, I-07100 Sassari, Italy
[d] Department of Inorganic Chemistry, Faculty of Pharmacy, Campus Cartuja, University of Granada, E-18071, Granada, Spain
[e] Laboratorio de Estudios Cristalográficos, IACT, CSIC-Universidad de Granada, Av. de las Palmeras 4, E-18100 Armilla, Granada, Spain
[f] Dipartimento di Scienze Chimiche e Farmaceutiche, Università di Ferrara, Via Fossato di Mortara 17, I-44121 Ferrara, Italy
[g] Faculty of Chemistry, University of Wroclaw, F. Joliot-Curie 14, Wroclaw, 50-383, Poland

Corresponding author: Valeria Marina Nurchi, Dipartimento di Scienze Chimiche e Geologiche, Cittadella Universitaria, 09042 Monserrato-Cagliari.
Phone +39 070 675 4476 Fax +39 070 675 4478 email: nurchi@unica.it

Keywords: Kojic acid, synthesis, hydroxypyrones, chelating agents, Fe^{3+}, Al^{3+}, Cu^{2+}, Zn^{2+}, thermodynamic measurements

Abstract

This work reports the synthesis, characterization and study of complex formation equilibria of four new bis-kojic acid chelators with Fe^{3+}, Al^{3+}, Cu^{2+} and Zn^{2+}. Based on previous encouraging results with tetradentate kojic acid derivatives, these ligands were designed with the aim of evaluating how acidic groups in the linker can affect both protonation constants and Fe^{3+} coordinating properties. Fe^{3+} and Al^{3+} complexation gave evidence of high metal-sequestering capacity, above all with the first metal ion. Complex formation equilibria with the essential metal ions Cu^{2+} and Zn^{2+} were furthermore studied to evaluate any disturbance of these chelating agents on the homeostatic equilibria of the essential metal ions. A multiplicity of techniques - potentiometry, UV–visible spectrophotometry, NMR spectroscopy and ESI–MS (electrospray ionization–mass spectrometry) - have enabled the characterization of the ligands, their corresponding metal complexes, together with an exhaustive analysis of the protonation and complex equilibria.

View Article Online
DOI: 10.1039/C7NJ03947F

Introduction

A relevant interest is addressed to the study of chelating agents for iron and aluminium, given that those nowadays in use, desferal, deferiprone and deferasirox, all present different drawbacks [1-4]. A number of chemical and biological requirements influence the design and synthesis of new ligands for chelation therapy[5]. The high stability of formed complexes is the first necessary, but not sufficient, requirement. In this perspective different ligands containing two kojic acid (KA) units joined by selected linkers were designed, synthesized, characterized by solid state X-ray diffraction and quantum chemical calculation, and their protonation and Al^{3+} and Fe^{3+} complex formation equilibria exhaustively studied with a variety of techniques (potentiometry, spectrophotometry, calorimetry, ESI-MS, NMR)[6-10]. The particular structure of the ligands gave rise to a noticeable increase in the stability of Al^{3+} and Fe^{3+} complexes with respect to that of the parent molecule KA. Among the synthetized ligands, those characterized by the shortest linkers (in Scheme 1) present the highest values both of pFe and pAl[111]. In particular, L3, bearing in the linker the vanillin residue, presents a particularly interesting chelating ability.

Acronym	Substituent R	pFe	pAl	Reference
L1	H	23.1	12.8	6
L2	*ortho*-vanillin	18.9	11.9	7
L3	vanillin	22.2	13.9	7
L8	CH_3	20.0	14.4	8

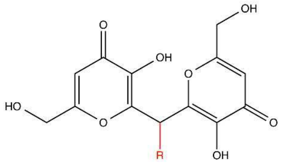

Scheme 1. Molecular structure of L1, L2, L3, L8 ligands[6-8].

We have synthesized a series of new molecules containing two different substituents R in the linker (Table 1) with the aim of evaluating how acidic groups in the linker affect both protonation constants and Fe^{3+} coordinating properties of the two KA moieties,. The substituents are a phenol moiety, characterized by a pK ~ 9, and a benzoic acid characterized by a pK ~ 4, one higher and the second lower than the pK of the OH group in KA. Furthermore, the acidic groups in the ring are either in ortho or in para position, the first allowing an easy formation of hydrogen bonds.

---

[1] pM is the parameter generally used to evaluate the overall stability of a chelating agent toward a given metal ion M. It is defined as the concentration, expressed as negative logarithm, of free metal ion in a solution at pH 7.4 that is 1 μM in the metal ion and 10 μM in the ligand.

View Article Online
DOI: 10.1039/C7NJ03947F

Table 1. Substituent (R), acronym and IUPAC name of L12-L15 compounds.

	Substituent R	Acronym	IUPAC name
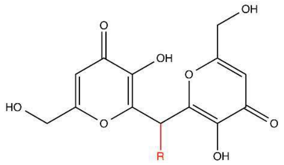	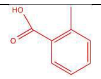	**L12**	2-{bis[3-hydroxy-6-(hydroxymethyl)-4-oxo-4*H*-pyran-2-yl]methyl}W benzoic acid
	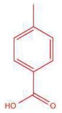	**L13**	4-{bis[3-hydroxy-6-(hydroxymethyl)-4-oxo-4*H*-pyran-2-yl]methyl} benzoic acid
	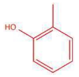	**L14**	2,2'-[(2-hydroxyphenyl)methanediyl]bis[3-hydroxy-6-(hydroxymethyl)-4*H*-pyran-4-one]
	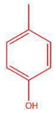	**L15**	2,2'-[(4-hydroxyphenyl)methanediyl]bis[3-hydroxy-6-(hydroxymethyl)-4*H*-pyran-4-one]

We present here the study of the protonation and complex formation equilibria of the four ligands with Fe^{3+} and Al^{3+} metal ions, and with the essential metal ions Cu^{2+} and Zn^{2+} [12-14]. As remarked in a speciation study showing that iron chelation could imply the depletion or dislocation of essential metal ions [15], a thorough study of copper and zinc complexation is of paramount importance and should always be presented for any ligand intended for use in therapy. The variety of substituents, besides acting on the binding properties, give to the ligands further properties (solubility, net charge at physiological pH, lipophilicity, etc.) that strongly affect a number of the requirements of a "good" iron chelator as absorption, bioavailability and excretion route [5]. After the synthesis and the characterization of the metal sequestering capacity, the further necessary steps on new chelating agents are the cellular and animal studies. The availability of a quantity of strong iron chelators with an assortment of biological properties will allow to better address these biotic studies.

Experimental

Materials

Kojic acid, NaOH, $AlCl_3$, $FeCl_3$, $CuCl_2$, $ZnCl_2$, HCl solution, NaCl, ethanol, ethyl acetate, dimethylamine, 2-formylbenzoic acid, 4-formylbenzoic acid, salicylaldehyde and 4-hydroxybenzaldehyde were purchased from Aldrich. All the reagents were used without further purification. Carbonate-free 0.1 M NaOH solution was prepared as previously described[16]. The

View Article Online
DOI: 10.1039/C7NJ03947F

metal ion standard solutions were prepared by dissolving the required amount of chloride salts in pure double distilled water and adding a stoichiometric amount of HCl to prevent hydrolysis. The solution of Fe^{3+} was standardized spectrophotometrically, using the formation of the colored Fe^{3+}-desferal complex, while EDTA titrations were used to standardized Al^{3+}, Cu^{2+} and Zn^{2+} solutions.

Synthesis

The synthesis were performed according to a described procedure[7] (Scheme 2).

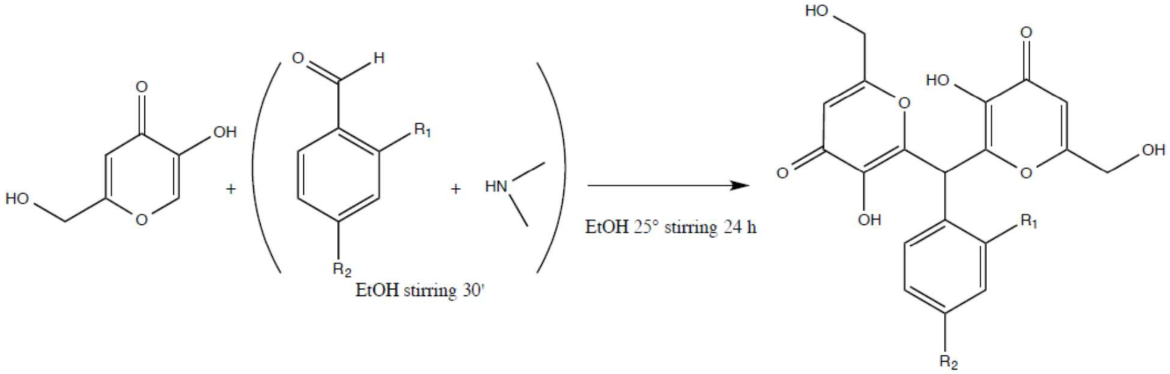

Scheme 2. Scheme of the synthesis of ligands: L12) R_1 = COOH, R_2 = H; L13) R_1 = H, R_2 = COOH; L14) R_1 = OH, R_2 = H; L15) R_1 = H, R_2 = OH.

L12 - 0.3970 g (3.53 mmol) of dimethylamine and 0.5255 g (3.50 mmol) of 2-formylbenzoic acid were dissolved in 2 ml of ethanol and stirred at room temperature for 30 min. The solution was added dropwise into 20 ml ethanolic solution of KA 1.0015 g (7.05 mmol). The reaction was carried out at room temperature for 24h; then the mixture was kept at -5C for 2h and the insoluble excess of substrate was filtered. The solvent was evaporated under reduced pressure, and the reaction product was dissolved in saturated sodium carbonate solution. After extraction with ethyl acetate, the water fraction was acidified with HCl 2M and above pH 3 a white precipitate appeared. The product was then filtered and washed with ethyl acetate and cold ethanol. Melting point 225ºC, yield 60.6 %, ESI–MS Found: 415.066 *m/z*; calculated 415.066 *m/z* for $(C_{20}H_{16}O_{10}\text{-}H)^-$, ^1H NMR (D_2O, 500 MHz) δ 4.31 (s, 4H, CH_2-OH), 6.49 (s, 2H), 6.71 (s, 2H), 7.28 (d, 1H), 7.41 (m, 2H), 7.67 (d, 1H).

L13 - 0.4045 g (3.27 mmol) of dimethylamine and 0.5032 g (3.35 mmol) of 4-formylbenzoic acid were dissolved in 2 ml of ethanol and stirred at room temperature for 30 min. The solution was added dropwise into 20 ml ethanolic solution of KA 1.0004 g (7.04 mmol). The reaction was carried out as described above. Melting point 250ºC, Analytical data: 62.7 % yield, ESI–MS Found: 417.074 *m/z*;

View Article Online
DOI: 10.1039/C7NJ03947F

calculated 417.082 *m/z* for $(C_{20}H_{16}O_{10}+H)^+$, ^{1}H NMR (D_2O, 500 MHz) δ 4.34 (s, 2H), 6.21 (s, 1H), 6.49 (s, 2H), 7.40 (d, 2H), 7.87 (d, 2H).

L14 - 0.4049 g (3.60 mmol) of dimethylamine and 0.4327 g (3.54 mmol) of salicylaldehyde were dissolved in 2 mL of ethanol and stirred at room temperature for 30 min. The solution was added dropwise into 20 ml ethanolic solution of KA 1.0106 g (7.11 mmol). The reaction was carried out as described above. Melting point 255ºC, yield 69.4 %, ESI–MS Found: 389.076 *m/z*; calculated: 389.082 *m/z* for $(C_{19}H_{16}O_9+H)^+$, ^{1}H NMR (D_2O, 500 MHz) δ 4.33 (s, 4H), 6.29 (s, 1H), 6.50 (s, 2H), 6.89 (m, 2H), 7.11 (d, 1H), 7.22 (t, 1H).

L15 - 0.4124 g (3.67 mmol) of dimethylamine and 0.4280 g (3.5 mmol) of 4-hydroxybenzaldehyde were dissolved in 2 mL of ethanol and stirred at room temperature for 30 min. The solution was added dropwise into 20 ml ethanolic solution of KA d 1.0842 g (7.6 mmol). The reaction was carried out as described above. Melting point 285ºC, yield 71.8 %, ESI–MS Found: 389.078 *m/z*; calculated 389.078 *m/z* for $(C20H16O10+H)^+$, ^{1}H NMR (D2O, 500 MHz) δ 4.36 (s, 4H), 6.07 (s, 1H), 6.48 (s, 2H), 6.82 (d, 2H), 7.22 (d, 2H).

The Figures S1, S2, S10, S11, S17, S18 and S25 in the Supplementary Material, reporting the ESI-MS spectra of the pure ligands, are indicative of their purity.

Potentiometric-spectrophotometric measurements

Protonation and complex formation equilibria were studied in a thermostatted glass cell, equipped with a magnetic stirrer, a Metrohm LL UNITRODE glass electrode connected to a Metrohm 691 pH-meter, a microburet delivery tube connected to a Dosimat 665 Metrohm titrator, an inlet–outlet tube for Argon and a fiber optic dip probe connected to a Varian Cary 50 UV–vis spectrophotometer. The electrode was calibrated daily in hydrogen ion concentration as previously described[17-19]. The calculations were performed with Hyperquad2013[20] [http://www.Hyperquad.co.uk/HQ2013.htm] and HypSpec2014[21] programs.

The protonation equilibria were studied at ligand concentration 5×10^{-4} M and the complex formation equilibria at a constant ligand concentration 5×10^{-4} M and 1:1, 1:2 and 1:3 metal/ligand molar ratios, ionic strength 0.1 M (NaCl). The samples were titrated with 0.1 M NaOH at 25.0˚C in the pH range 2.0–11. Protonation and iron complex formation equilibria were studied using a previously described combined spectrophotometric-potentiometric procedure[22]. Standard deviations (s values) computed by Hyperquad and HypSpec refer to random errors only. They are, however, a

View Article Online
DOI: 10.1039/C7NJ03947F

good indication of the importance of the particular species involved in the equilibrium. Log β_{pqr} values refer to the overall equilibria $p\mathrm{M} + q\mathrm{H} + r\mathrm{L} \leftrightarrows \mathrm{M}_p\mathrm{H}_q\mathrm{L}_r$ (electrical charges omitted), and L represents the completely deprotonated ligand.

NMR

NMR experiments were carried out on a Bruker Ascend$^{\mathrm{TM}}$ 400 MHz spectrometer (Bruker, Billerica, MA, USA) equipped with a 5 mm automated tuning and matching broad band probe (BBFO) with z-gradients, as previously described [23-25]. NMR measurements were performed by using a concentration of the ligands of 5-7 mM, in 90/10 (*v*/*v*) H_2O/D_2O, at 25˚C in 5 mm NMR tubes. The solvent suppression in the 1D ^{1}H experiments was performed by using excitation sculpting with gradients. All NMR data were processed by using TopSpin (Bruker Instruments) software and analyzed by using Sparky 3.11 and MestRe Nova 6.0.2 (Mestrelab Research S.L.) programs (Santiago de Compostela, Spain), as already reported [10, 25-29].

Calorimetry for protonation equilibria

$\Delta H°$ e $\Delta S°$ values were obtained with calorimetric titrations on a Tronac 450 calorimeter equipped with a 25 mL Dewar titration vessel; the titrant solution was added using a 2 mL Hamilton syringe also immersed in the thermostatic bath. A warming resistance (about 100 Ω) and a thermistor put into the sample solution allowed the instrument electric calibration and the detection of temperature variations, respectively. The accuracy of the system was checked daily by titrating a tris(hydroxymethyl)aminomethane solution, partially neutralized with hydrochloric acid. The thermostatic bath was at 25.00 ± 0.02 °C. Home-made programs were used to manage the completely automated system, *via* Tronac 900 interface, to collect and store the rough calorimetric data, and for gross heat correction from non-chemical factors and from the dilution heats, determined by means of separate experiments[30]. The difference of potential given by the thermistor was measured by a digital multimeter (FLUKE 8840A). The ionic strength was adjusted at 0.1 M with KCl. $\Delta H°$ values were computed from the calorimetric data by means of the least-squares computer program HypDH[31], which minimizes the function $U = \Sigma w_\mathrm{i}(Q_\mathrm{i}^\mathrm{o} - Q_\mathrm{i}^\mathrm{c})^2$, where w_i are statistical weights and Q_i^o, Q_i^c are the experimental and calculated heats, respectively. Concerning water, the literature $\Delta H°_\mathrm{w}$ value of 56.4 kJ mol^{-1} was used in the calculations[32]. $\Delta S°$ values were computed from corresponding $\Delta H°$ values by means of the Gibbs-Helmholtz equation: $-\Delta G° = -$

View Article Online
DOI: 10.1039/C7NJ03947F

$\Delta H°$ + $T\Delta S°$; the free energy variation ($\Delta G°$) was calculated by the corresponding cumulative constants (β), given by potentiometry and/or spectrophotometry, through the relationship: $-\Delta G° = 2.303\ RT \log \beta$.

Electrospray ionization-mass spectrometry (ESI-MS)

High-resolution mass spectra were performed using a Bruker MicrO-TOF-Q spectrometer (Bruker Daltonik, Bremen, Germany), equipped with an Apollo II electrospray ionization source with an ion funnel. The spectra were recorded in the positive and negative ion modes in the range 100 to 1500 *m/z*. The instrument parameters were: dry gas–nitrogen, temperature 200 °C, ion source voltage 4500 V, collision energy 10 eV. Analyte aqueous solutions (70 µl) were introduced at a flow rate of 3 µl/min. Stock solutions were prepared by using MeOH/H_2O mixture (50/50 v/v) as a solvent. The metal to ligand molar ratio was 1:1. The final pH of the solution was 4.0. The instrument was calibrated using the Tunemix mixture (BrukerDaltonik, Germany) in the quadratic regression mode. The overall charge of the analyzed ion was calculated on the base of distance between isotopic peaks. Data were processed by application of the Compass DataAnalysis 4.0 (Bruker Daltonik, Germany) program[33].

Results and discussion

Protonation equilibria.

The protonation equilibria of the four ligands were studied by a joined potentiometric-spectrophotometric technique[34], by ^1H NMR spectroscopy and calorimetry. The joined potentiometric-spectrophotometric measurements for L12-L15 ligands allowed the calculation of the protonation constants related the three steps with the aid of the Hyperquad and HypSpec programs. The protonation constants, together with the corresponding thermodynamic parameters ($\Delta G°$, $\Delta H°$ and $T\Delta S°$), evaluated by calorimetric measurements, are reported in Table 2. The equivalent literature values for L2 and L3 ligands are also reported in order to have a more complete picture of the effects of the substituents[7]. Figure 1 reports the speciation plots of the four ligands.

View Article Online
DOI: 10.1039/C7NJ03947F

Table 2. Thermodynamic parameters for the protonation of the ligands L12-L15; the corresponding data for L2 and L3 are also reported for the sake of comparison[7]. The data related to the protonations in the KA units are in bold characters.

Ligand	**log*K***	**$-\Delta G^\circ$ (kJ mol^{-1})**	**$-\Delta H^\circ$ (kJ mol^{-1})**	**$T\Delta S^\circ$ (kJ mol^{-1})**
L12	**9.57 (3)**	**54.6 (1)**	**18.8 (6)**	**35.8 (6)**
	7.44 (2)	**42.4 (1)**	**12 (1)**	**30 (1)**
	3.49 (1)	19.9 (1)	-1.3 (8)	21.2 (8)
L13	**9.24 (2)**	**52.7 (1)**	**15.1 (6)**	**37.6 (6)**
	7.04 (3)	**40.2 (1)**	**11.3 (6)**	**28.9 (6)**
	4.14 (1)	23.6 (1)	1.3 (4)	22.3 (4)
L14	10.10 (3)	57.6 (1)	25 (1)	33 (1)
	8.57 (1)	**48.9 (1)**	**20 (1)**	**29 (1)**
	6.91 (1)	**39.4 (1)**	**14 (1)**	**25 (1)**
L15	9.98 (2)	56.9 (1)	14.6 (6)	42.3 (6)
	8.47 (2)	**48.3 (1)**	**17 (1)**	**31 (1)**
	6.78 (1)	**38.7 (1)**	**12 (1)**	**27 (1)**
L2 [a]	10.58 (3)	60.4 (2)	0 (1)	60 (1)
	8.92 (2)	**50.9 (1)**	**14 (1)**	**37 (1)**
	6.95 (1)	**39.6 (1)**	**12 (2)**	**28 (2)**
L3 [a]	10.18 (2)	58.1 (3)	12 (1)	46 (1)
	8.84 (1)	**50.4 (1)**	**16 (1)**	**34 (1)**
	7.21 (1)	**41.1 (1)**	**12 (1)**	**29 (1)**

< Fig. 1>

Figure 1. Speciation plots of the four ligands A) L12, B) L13, C) L14 and D) L15. The speciation plots of the species related to protonation of KA units are dashed lines.

View Article Online
DOI: 10.1039/C7NJ03947F

Furthermore, spectrophotometric measurements permit an easy attribution of the protonation steps that involve KA moieties, because the different spectral features of protonated and ionized forms of KA. The deprotonated L^- species presents a band at 315 nm (ε = 5900 $M^{-1}cm^{-1}$) while the protonated LH form is characterized by a more intense band at 270 nm (ε = 8700 $M^{-1}cm^{-1}$)[6].

< Fig. 2>

Figure 2. Absorptivity spectra of various protonated forms of L12 ligand.

We will discuss the absorptivity spectra of the different species of L12 (Figure 2), calculated by HypSpec2014 program[21] from the spectra collected during the base titration, as representative of the behavior of all the studied ligands. Ligand L12, in its deprotonated form L^{3-}, is characterized by a band at 335 nm (ε = 10100 $M^{-1}cm^{-1}$) of intensity, almost double than that of KA, due to the contribution of two similar chromophore units. Passing to the mono-protonated form LH^{2-}, the band at 335 nm undergoes a slight blue shift (~ 324 nm), its intensity is halved, and a new band appears at 280 nm. In the second protonation step, the band at 324 nm disappears and the band at 280 nm nearly doubles in intensity. The third protonation step does not present appreciable spectral variations. Based on the above observations, the first two steps are attributed to the protonation of the O^- groups in KA units, and the third, spectrally silent, to that of the carboxylate group.

The protonation steps of each ligand were followed in a detailed way by ^1H NMR titrations. NMR measurements confirm the numerical values of protonation constants and their attribution to the functional groups involved in each protonation step. Furthermore, the trend of chemical shifts of the various protons vs pH, discussed in a detailed way in the Supplementary Material (S1-NMR Protonation sequence), permits one to envisage a possible sequence of intramolecular hydrogen bond forming and breaking that can be of aid in the rationalization of thermodynamic results.

A small but significant difference in the thermodynamic parameters for the first protonation step is observed between L12 and L13 (about 0.3 logK units, and 2 kJ mol^{-1} in $-\Delta G°$, Table 2). This difference is due to a more favourable enthalpic term for L12, while a smaller but opposite trend can be observed for the entropic contribution. In both cases a hydrogen bond forms between the protonated OH in one KA unit and the O^- group in the other, but at the expense of two previous hydrogen bonds between O^- and CH_2OH and between COO^- and CH_2OH in the anonic L^{3-} form of L12, and of a single hydrogen bond between O- and CH_2OH in L13.

View Article Online
DOI: 10.1039/C7NJ03947F

The second protonation implies in both L12 and L13 the breaking of the hydrogen bond between O^- in one KA unit and OH in the second unit. However, a new hydrogen bond can form between one OH group on the KA units and the COO- group, and this can account for the higher logK_2 (0.4 logK units) and 2 kJ mol-1 in –ΔG°, for the protonation of the second O^- group in KA unit in L12 with respect of L13. In this case, both enthalpic and entropic terms play to favor the protonation of L12 with respect to L13.

The logK_3 value of L12 (protonation of carboxylate group) is lower (0.65 units) than that of L13. This depends on the hydrogen bond between COO- and the OH group in one KA unit, not possible in L13. This is supported by the comparison of thermodynamic protonation data of Table 2, with the corresponding literature parameters for free benzoic acid under similar experimental conditions (log$K$ = 3.99, -ΔH° = 0.87 kJ·mol^{-1}, TΔS° = 21.9 kJ·mol^{-1})[35]. The protonation of the carboxylate group of L12 is characterized by a less favorable ΔG° value while ΔH° becomes endothermic, in agreement with the suggested break of the H-bond requested for carboxylate protonation. On the other hand, the TΔS° value is only slightly influenced by the presence of the hydrogen bond since it is mainly due to variations in the hydration spheres that, in turn, essentially depend on the charge variations during the process. In L13, instead, all the thermodynamic parameters referring to carboxylate protonation are very similar to those reported for free benzoic acid, in agreement with the observation that no H-bond is possible between the carboxylate group and the rest of the molecule.

As far as L14 and L15 are concerned, the phenolate group O^- in the substituent is the most basic group, characterized by the logK_1 values 10.10 and 9.98 in L14 and L15 respectively, slightly higher than the value 9.79 of pure phenol in similar conditions[34]. Rather surprisingly, the possible hydrogen bond formation between the phenolic group in L14 and the O- group on one KA unit acts only a minor role in determining the logK_1 values that are almost similar in the two ligands. However, thermodynamic data of Table 2 show that this behaviour is the result of the enthalpic-entropic compensation. In fact,the enthalpic term measured for L14 (25 kJ·mol^{-1}) is significantly higher than that obtained for L15 (15 kJ·mol^{-1}), supporting the hypothesis of the presence of a hydrogen bond which, on the other hand, causes that the corresponding entropic contributions have an opposite trend. The logK_2 and logK_3 values for L14 and L15 relative to the KA unit protonation are noticeably lower than the corresponding logK_1 and logK_2 values measured for L12 and L13 (1.0-0.8 and 0.5-0.3 units, respectively), essentially for enthalpic reasons. This difference can be ascribed to the overall different charge of the ligands due to COO^- and OH groups in the substituent.

View Article Online
DOI: 10.1039/C7NJ03947F

An analogous trend was observed for the log*K* values of L2 and L3, even if the OCH_3 always in *orto* with respect to OH group makes it more basic for its marked inductive effect [34].

Complex formation equilibria with Fe^{3+}.

The intense visible bands of the Fe^{3+} complexes allowed the study of their formation equilibria by joined potentiometric-spectrophotometric titrations. The spectra were collected in the range 300 – 700 nm, after each addition of a known volume of base solution. In a limited pH interval (4.5-5.5), the iron complex formed a precipitate that then completely dissolved. When Fe^{3+} and ligands were mixed (pH about 2) the complex formation was almost complete. This required the collection of additional spectra by addition of hydrochloric acid until disappearance of the signals of complexes (pH range 0 – 2). As an example, selected spectra for the Fe^{3+}/L15 system are shown in Figure 3. The similarity of the obtained spectra with those of the complex $[Fe(KA)_2]^+$ [6], led us to hypothesize the formation of a binuclear $Fe_2L_2H_2$ complex in which each iron ion is coordinated by two KA units, being the two protons on the phenolic groups of the two substituents. The heights of the band at around 500 nm were calculated by a spectral decomposition procedure[36]. When plotted *vs* pH, they allowed a preliminary evaluation of the stability constant of the $[Fe_2L_2H_2]^{2+}$ complex, successively refined with HypSpec2014 program (Table 3). The potentiometric data of the titration in 2-11 pH range, processed by Hyperquad2013 program[37], with the logβ of $[Fe_2L_2H_2]^{2+}$ fixed, allowed us to identify the complexes reported in Table 3, and to evaluate the related formation constants.

Table 3. Stability constants of Fe^{3+} complexes with the ligands L12-L15, calculated with HypSpec2014 and Hyperquad2013 programs at 25°C and 0.1 M (NaCl) ionic strength. The calculated pFe values are in the lower row.

	L12		**L13**		**L14**		**L15**	
Model	logβ	pK	logβ	pK	logβ	pK	logβ	pK
$[Fe_2L_2H_2]^{2+}$	47.72 (3)		47.42 (4)		57.78 (5)		57.39 (2)	
$[Fe_2L_2H]^+$	44.23 (6)	3.49	--	3.09	53.42 (6)	4.36	53.15 (6)	4.24
Fe_2L_2	40.09 (3)	4.14	41.60 (5)	3.09	48.61 (5)	4.81	48.41 (5)	4.74
$[Fe_2L_2H_{-1}]^-$	34.31 (4)	5.78	36.28 (5)	5.21	42.95 (4)	5.66	41.13 (4)	7.28]
$[Fe_2L_2H_{-2}]^{2-}$	28.13 (3)	6.18	30.06 (4)	6.25	35.14 (3)	7.81	--	--
$[Fe_2L_2H_{-3}]^{3-}$	--	--	22.42 (4)	7.66	--	--	--	--

View Article Online
DOI: 10.1039/C7NJ03947F

$[Fe_2L_2H_{-4}]^{4-}$	--	--	12.35 (6)	10.07	--	--	--	--
pFe	17.1		18.6		19.3		18.7	

Only binuclear complexes of general stoichiometry $[Fe_2L_2H_r]$ are formed. Negative values of r identify hydroxo complexes.

< Fig.3>

Figure 3. Representative spectra of the acid titration of Fe^{3+}/L15 system at 1:1 Fe$^{3+:}$L molar ratio, [L15] = $4.29 \cdot 10^{-4}$ M, and different pH values (pH 0.12 lower spectrum, pH 2.73 higher spectrum).

The ESI-MS measurements support these findings; the results in Table 4 confirm for all four ligands the formation of positively charged binuclear iron complexes with up to three coordinated water molecules. The ESI-MS spectra of iron complexes are reported in Supplementary Material in the Figures specified in Table 4.

Table 4. ESI-MS results for iron complexes.

Fe-L12			Fe-L13		
m/z	Complex	Figure	*m/z*	Complex	Figure
466.973	$[Fe_2(L12_{ox})_2H_2]^{2+}$	S6	469.995	$[Fe_2(L13)_2H_2]^{2+}$	S15
475.976	$[Fe_2(L12_{ox})H_2+H_2O]^{2+}$		478.998	$[Fe_2(L13)_2H_2+H_2O]^{2+}$	
484.991	$[Fe_2(L12_{ox})_2H_2+2H_2O]^{2+}$		488.004	[Fe2(L13)2H2+2H2O]2+	
493.980	$[Fe_2(L12_{ox})_2H_2+3H2O]^{2+}$				
1040.870	[Fe2(L12ox)2H2+3Cl]-	S7			
Fe-L14			Fe-L15		
m/z	Complex	Figure	*m/z*	Complex	Figure
441.996	$[Fe_2(L14)_2H_2]^{2+}$	S22	441.991	$[Fe_2(L15)_2H_2]^{2+}$	S27
450.992	$[Fe_2(L14)_2H_2+H_2O]^{2+}$		450.998	[Fe2(L15)2H2+H2O]2+	
460.001	$[Fe_2(L14)_2H_2+2H_2O]^{2+}$		460.004	$[Fe_2(L15)_2H_2+2H_2O]^{2+}$	

< Fig.4>

Figure 4. Speciation plots of iron complexes with the four ligands A) L12, B) L13, C) L14 and D) L15, calculated using the stability constants in Table 3, at ligand and Fe^{3+} concentration $1 \cdot 10^{-3}$ M.

View Article Online
DOI: 10.1039/C7NJ03947F

The speciation plots of iron complexes (Figure 4) permit some structural considerations. The starting $[Fe_2L_2H_2]^{2+}$ complex with L12 can be hypothesized as a binuclear complex in which each Fe^{3+} ion is coordinated by two KA units from two different ligands *via* the oxygen atoms, the hexa-coordination being completed by two water molecules. The two carboxylic groups in the linker are still protonated (Scheme 3 A). They lose their protons with pK 3.49 and 4.14, the first equal to that of the free ligand and the second slightly higher, although lower values were presumably due to the entire molecule positively charged. This can be rationalized, taking into account that the low pK values of carboxylic group in free L12 were determined by the stabilizing effect of the hydrogen bond between carboxylate and the OH group in KA moiety. This is not anymore possible in the complexed ligand being the deprotonated O^- group involved in iron coordination. The formation of the neutral complex Fe_2L_2 between pH 4 and 5 leads to precipitation. Increasing the pH, two of the coordinated water molecules lose their protons with pK 5.78 and 6.18 respectively, leading to the soluble negatively charged complex $[Fe_2L_2H_{-2}]^{2-}$, the prevailing form at physiological pH. A pFe value 17.1 defines the chelating ability of L12 toward Fe^{3+}.

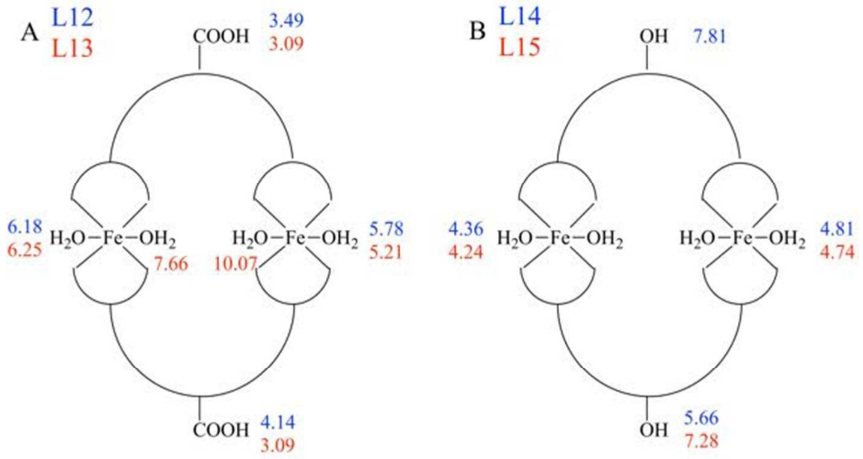

Scheme 3. Hypothesized coordination scheme of L12-L15 ligands with Fe^{3+}. The pK values for the loss of protons from the different groups are reported in blue for L12 and L14, and in red for L13 and L15.

The coordination scheme of L13 with Fe^{3+} is similar to that of L12, but the two carboxylic protons are lost together with pK 3.09, lower than the corresponding values for L12. In this case, the positive charge of the entire molecule favours the deprotonation of the carboxylic groups as expected. Furthermore, the neutral complex Fe_2L_2 with L13 loses up to four protons from the

View Article Online
DOI: 10.1039/C7NJ03947F

coordinated water molecules, the first two with pK 5.21 and 6.25 and the remaining two with pK 7.66 and 10.07. The prevailing species at pH 7.4 is always $[Fe_2L_2H_{-2}]^{2-}$ (Figure 4), accompanied by a non-negligible amount of $[Fe_2L_2H_{-3}]^{3-}$. The pFe value 18.7, higher than that of L12, depends both on the lower protonation constants and on the higher complex formation constants (Tables 2 and 3). As regards L14 and L15, the deprotonation of the coordinated water molecules takes place with lower pK values (4.26 and 4.81 for L14, and 4.24 and 4.74 for L15), due to the starting molecule being positively charged. The following pK's (two for L14 and one for L15) are difficult to be attributed, due to the possibility that the protons are lost either from further coordinated water molecules or from the phenolic group on the linker. The prevailing species at pH 7.4 are the negative $[Fe_2L_2H_{-1}]^-$ in the case of L14 (pFe^{3+} 19.3) and the neutral Fe_2L_2 in the case of L15 (pFe^{3+} 18.7).

Complex formation equilibria with Al^{3+}, Cu^{2+} *and* Zn^{2+}.

The complex formation equilibria of the four ligands with Al^{3+}, Cu^{2+} and Zn^{2+} have been studied by potentiometric methods and ESI-MS. The formed complexes and their formation constants are reported in Table 5, and the related speciation plots in Figure 5. Al^{3+} forms complexes similar to those with iron, but of lower stability. A mononuclear complex $[AlL_2H_2]^{2+}$ forms with L12 at low pH, in which one Al^{3+} ion is coordinated by two KA units of two different ligands, the two carboxylic groups are deprotonated and the two OH groups on the non-coordinating KA moieties are protonated. This complex at pH 5 binds a second Al^{3+} ion, giving the neutral binuclear Al_2L_2 complex. The first formed complex with L13 is the binuclear $[Al_2L_2H]^+$ still protonated on a carboxylic group. The binuclear aluminium complexes with L12 and L13 at increasing pH give rise to hydroxo complexes, similar to those observed with iron. The prevailing species at physiological pH are $[Al_2L_2H_{-1}]^-$ and $[Al_2L_2H_{-2}]^{2-}$ in different ratios (Figure 5) and the pAl^{3+} values are 12.3 and 12.2 for L12 and L13 respectively (Table 5). L14 and L15 behave with Al^{3+} in an analogous way to that observed with iron.

The prevailing species at pH 7.4 are also in this case $[Al_2L_2H_{-1}]^-$ and $[Al_2L_2H_{-2}]^{2-}$ in different ratios and the pAl3+ values are 13.1 and 13.2 for L14 and L15 respectively, about one unit higher than the corresponding values with L12 and L13.

View Article Online
DOI: 10.1039/C7NJ03947F

Table 5. Stability constants of Al^{3+} complexes with the ligands L12-L15, calculated with Hyperquad2013 program at 25°C and 0.1 M (NaCl) ionic strength. The related pAl values are in the lower row.

	L12		**L13**		**L14**		**L15**	
Model	logβ	pK	logβ	pK	logβ	pK	logβ	pK
$[Al_2L_2H_2]^{2+}$	-----		----		48.58 (6)		48.6 (1)	
$[Al_2L_2H]^{+}$	-----		34.96 (6)		43.65 (6)	4.93	43.0 (1)	5.6
Al_2L_2	30.81 (4)		30.26 (6)	4.70	37.57 (7)	6.08	37.73 (5)	5.3
$[Al_2L_2H_{-1}]^{-}$	----		24.57 (5)	5.69	30.45 (5)	7.12	29.7 (1)	8.0
$[Al_2L_2H_{-2}]^{2-}$	18.09 (4)	6.36	17.08 (7)	7.49	----		----	
$[Al_2L_2H_{-3}]^{3-}$	9.89 (5)	8.20	8.90 (6)	8.18	----		----	
$[AlL_2H_2]^{-}$	35.95 (5)		----		----		----	
pAl	12.3		12.2		13.1		13.2	

< Fig.5>

Figure 5. Speciation plots of aluminium complexes with the four ligands A) L12, B) L13, C) L14 and D) L15, calculated using the stability constants in Table 6, at ligand and Al^{3+} concentration $1\cdot10^{-3}$ M.

The ESI-MS results substantiate these findings. The results reported in Table 6 confirm for L12, L13 and L14 ligands the formation of positively charged binuclear aluminium complexes with up to two coordinated water molecules. Binuclear aluminium complexes were also observed in the negative mode ESI-MS spectrum. Complexes of higher stoichiometry were furthermore detected, but in negligible amounts. The collection of ESI-MS spectra with L15 ligand gave unreliable results, not reported here. The ESI-MS spectra of aluminium complexes are reported in Supplementary Material in the Figures specified in Table 6.

View Article Online
DOI: 10.1039/C7NJ03947F

Table 6. ESI-MS results for aluminium complexes.

Al-L12			Al-L13		
m/z	Complex	Figure	*m/z*	Complex	Figure
441.035	$[Al_2(L12)_2H_2]^{2+}$	S3	441.029	$[Al_2(L13)_2H_2]^{2+}$	S12
440.027	$[Al_2(L12_{ox})_2H_2]^{2+}$				
450.041	$[Al_2(L12)_2H_2 + H_2O]^{2+}$				
459.045	$[Al_2(L12)_2H_2 + 2H_2O]^{2+}$		459.040	$[Al_2(L13)_2H_2{+}2H_2O]^{2+}$	
449.033	$[Al_2(L12ox)_2H_2 + H_2O]^{2+}$				
458.038	$[Al_2(L12ox)_2H_2 + 2H_2O]^{2}$				
474.999	$[Al_2(L12)_2 + 2Cl]^{2-}$	S4			
915.036	$[Al_4(L12)_4{+}2Cl]^{2-,}$				
933.022	$[Al_4(L12)_4{+}2Cl{+}2H_2O]_{2-}$				
951.009	$[Al_4(L12)_4{+}2Cl{+}4H_2O]^{2-}$				
Al-L14			Al-L15		
m/z	Complex	Figure	*m/z*	Complex	Figure
413.038	$[Al_2(L14)_2H_2]^{2+}$	S19			
422.044	$[Al_2(L14)_2H_2{+}H_2O]^{2+}$				
431.049	$[Al_2(L14)_2H_2{+}2H_2O]^{2+}$				
607.077	$[Al_2(L14)_3H_5]^{2+}$				
422.049	$[Al_2(L14)_2H_2{+}H_2O]^{2+}$	S20			
431.056	$[Al_2(L14)_2H_2{+}2H_2O]^{2+}$				

The stability constants for Cu^{2+} (Table 7) and the related speciation plots (Figure 6) permit the description of the complex formation sequence as a function of pH. Cu^{2+} forms with L12 and L13, in the acidic pH range 2-3, a binuclear complex $[Cu_2LH]^{2+}$, in which a ligand molecule binds two copper ions, one with each KA moiety. This complex transforms into a $[Cu_2L_2H]^-$ that loses a proton with pK's 5.31 and 5.95 for L12 and L13, giving a $[Cu_2L_2]^{2-}$ complex. These pK values appear too high (~two units higher than in the free ligand) to be attributed to the deprotonation of a carboxylic group, even taking into account the negative charge of the entire molecule. A further possibility is that in $[Cu_2L_2H]^-$ one copper ion is coordinated by two KA units and the second by one, being the

View Article Online
DOI: 10.1039/C7NJ03947F

remaining still protonated on the OH group. This complex transforms into the $[Cu_2L_2]^{2}$, where both copper ions are coordinated by two KA units.

Table 7. Stability constants of Cu^{2+} complexes with the ligands L12-L15, calculated with Hyperquad2013 program at 25°C and 0.1 M (NaCl) ionic strength. The related pCu values are in the lower row.

	L12		**L13**		**L14**		**L15**	
Model	logβ	pK	logβ	pK	logβ	pK	logβ	pK
$[CuLH_2]^+$	-----		----		25.34 (5)		24.9 (1)	
CuLH	-----		----		----		----	
$[Cu_2LH]^{2+}$	22.62 (4)		20.89 (4)		----		----	
$Cu_2L_2H_2$	----		----		44.84 (2)		45.14 (6)	
$[Cu_2L_2H]^-$	35.10 (2)		32.31 (3)		38.68 (3)	6.16	----	
$[Cu_2L_2]^{2-}$	29.79 (1)	5.31	26.36 (5)	5.95	31.89 (5)	6.79	33.14 (7)	6.00
$[Cu_2L_2H_{-1}]^{3-}$	23.48 (3)	6.31	20.17 (3)	6.19	21.3 (1)	10.39	23.8 (2)	9.3
$[Cu_2L_2H_{-2}]^{4-}$	14.17 (2)	9.31	----		----		----	
pCu	11.1		9.9		10.1		10.9	

The complex with L12 loses two further protons from the coordinated water molecules with pK 6.31 and 9.31, and that with L13 one proton at 6.19. The prevailing species at pH 7.4 is the $[Cu_2L_2H_{-1}]^{3-}$ complex that determines pCu values 11.1 and 9.9 for L12 and L13, respectively.

< Fig.6>

Figure 6. Speciation plots of copper complexes with the four ligands A) L12, B) L13, C) L14 and D) L15, calculated using the stability constants in Table 7, at ligand and Cu^{2+} concentration $1\cdot10^{-3}$ M.

The L14 and L15 ligands form with copper the mononuclear $[CuLH_2]^+$ complex where Cu^{2+} is coordinated by one KA unit, being the second still protonated as well as the phenolic group on the linker. This $[CuLH_2]^+$ complex transforms in the $Cu_2L_2H_2$ binuclear neutral complex that loses two protons from the coordinated water molecules with pK's 6.16 and 6.79 from L14 and with the same pK 6.00 from L15, then from one phenolic group with pK 10.6 and 9.3 from L14 and L15

View Article Online
DOI: 10.1039/C7NJ03947F

respectively. The prevailing species at pH 7.4 are $[Cu_2L_2H]^-$ and $[Cu_2L_2]^{2-}$ for L14 and $[Cu_2L_2]^{2-}$ for L15, determining the pCu values 10.1 and 10.9 respectively.

The ESI-MS spectra of the four ligands with copper are characterized by the presence of the few peaks in Table 8. However, the formation of binuclear positively charged complexes is confirmed by this technique. The ESI-MS spectra of copper complexes are reported in Supplementary Material in the Figures specified in Table 8.

Table 8. ESI-MS results for copper complexes.

Cu-L12			Cu-L13		
m/z	Complex	Figure	*m/z*	Complex	Figure
475.974	$[Cu(L12_{ox})H_2]^+$ $[Cu_2(L12_{ox})_2H_4]^{2+}$	S5	477.986	$[Cu(L13)H_2]^+$ $[Cu_2(L13)_2H_4]^{2+}$	S14
493.990	$[Cu(L12_{ox})H_2+H_2O]^+$		954.960	$[Cu_2(L13)_2H]^+$	
Cu-L14			Cu-L15		
m/z	Complex	Figure	*m/z*	Complex	Figure
449.991	$[Cu(L14)H_2]^+$ $[Cu_2(L14)_2H_4]^{2+}$	S21	389.078,	$[(L15)H_3+H]^+$	S26
838.061	$[Cu(L14)_2H_5]^+$		449.995	$[Cu(L15)H_2]$+ $[Cu2(L15)2H_3]^{2+}$	
898.972	$[Cu_2(L14)_2H_3]^+$		898.983	$[Cu_2(L15)_2H_3]^+$	
			920.976	$[Cu_2(L15)_2H_2+Na]^+$	

The first complex formed by Zn^{2+} with L12 and L13 is the binuclear complex $[Zn_2LH]^{2+}$: each metal ion is coordinated by one KA unit on the same molecule, being the carboxylic group still protonated. The $[Zn_2LH]^{2+}$ complex with L12 transforms into a $[Zn_2L_2]^{2-}$ species, in which each zinc ion is coordinated by two KA units being the carboxylic groups deprotonated. The $[Zn_2LH]^{2+}$ complex with L13 transforms into a $[Zn_2L_2H]^-$ complex, and then to a $[Zn_2L_2]^{2-}$ form with pK 6.1. This value is too high to be attributed to a carboxylic group, even taking into account the negative charge on the molecule. We can hypothesize a form in which both carboxylic groups are deprotonated, one Zn^{2+} ion is coordinated by two KA moieties, and the second only by one KA unit, being the second still protonated but not implied in bonding. The pK 6.1 thus corresponds to the loss of this proton, with the bonding of zinc by the second KA unit.

View Article Online
DOI: 10.1039/C7NJ03947F

< Fig.7>

Figure 7. Speciation plots of zinc complexes with the four ligands A) L12, B) L13, C) L14 and D) L15, calculated using the stability constants in Table 9, at ligand and Zn^{2+} concentration $1 \cdot 10^{-3}$ M.

A final deprotonation occurs both in L12 and L13 giving the hydroxo-complex $[Zn_2L_2H_{-1}]^{3-}$ with pK 7.5 and 8.9 for L12 and L13 respectively. The prevailing species at pH 7.4 are with L12 $[Zn_2L_2]^{2-}$ and $[Zn_2L_2H_{-1}]^{3-}$ in similar amounts, giving a pZn 7.5, and $[Zn_2L_2]^{2-}$ with L13 giving a lower pZn 6.8. With the L14 and L15 ligands, the first formed complex is the neutral $[Zn_2L_2H_2]$ that in the case of L14 loses two protons from the coordinated water molecules with pK 6.5, 0.4 units lower than in the free ligand, and in L15 only one proton with pK 7.5. Deprotonation of phenolic protons at high pH values was not observed. At pH 7.4 the species $[Zn_2L_2]^{2-}$ exists in L14, and $[Zn_2L_2H_2]$ and $[Zn_2L_2H]^{-}$ In L15, giving respectively the pZn values 7.7 and 6.4.

Table 9. Stability constants of Zn^{2+} complexes with the ligands L12-L15, calculated with Hyperquad2013 program at 25°C and 0.1 M (NaCl) ionic strength. The related pZn values are reported in the lower row.

	L12		**L13**		**L14**		**L15**	
Model	logβ	pK	logβ	pK	logβ	pK	logβ	pK
$[Zn_2LH]^{2+}$	19.3 (2)		18.6 (1)		----		----	
$Zn_2L_2H_2$	----		----		40.0 (1)		38.3 (1)	
$[Zn_2L_2H]^{-}$	----		27.2 (1)		----		30.8 (1)	7.5
$[Zn_2L_2]^{2-}$	23.5 (1)		21.1 (1)	6.1	27.1 (2)	6.5	----	
$[Zn_2L_2H_{-1}]^{3-}$	16.0 (1)	7.5	12.2 (1)	8.9	----		----	
pCu	7.1		6.7		7.7		6.4	

ESI-MS spectra for the reaction between Zn^{2+} and the four ligands are characterized by intense signals of free ligand, due to the low stability of zinc complexes. The presence of signals from positively and negatively charged mononuclear complexes, and positively charged binuclear complexes, except with L12 ligand, is also observed. The ESI-MS spectra of zinc complexes are reported in Supplementary Material in the Figures specified in Table 10.

View Article Online
DOI: 10.1039/C7NJ03947F

Table 10. ESI-MS results for zinc complexes.

Zn-L12			Zn-L13		
m/z	Complex	Figure	*m/z*	Complex	Figure
476.972	$[Zn(L12_{ox})H_2]^+$	S8	478.988	[Zn2(L13)2H4]2+ [Zn(L13)H2]+	S16
478.979	$[Zn(L12)H_2]^+$		496.998	$[Zn(L13)H_2+H_2O]^+$	
477.096	$[Zn(L12)]^-$	S9	514.977	$[Zn(L13)H_2+2H_2O]^+$	
512.952	$[Zn(L12)H+Cl]^-$				
548.920	$[Zn(L12)H_2+2Cl]^-$				
Zn-L14			Zn-L15		
m/z	Complex	Figure	*m/z*	Complex	Figure
450.990	$[Zn_2(L14)_2H_4]^{2+}$ $[Zn(L14)H_2]^+$	S23	450.995	$Zn(L15)H_2]^+$ $[Zn_2(L15)_2H_4]^{2+}$	S28
469.004.	$[Zn(L14)H_2+H_2O]^+$		469.006	$[Zn(L15)H_2+H_2O]^+$	
			486.977	$[Zn(L15)H_2+2H_2O]^+$	

Conclusions

Some conclusive remarks have to be pointed out on the effect of the substituents in the aromatic ring both on the protonation constants and on the pM values with the four metal ions.

The first protonation constant on KA units is highly enhanced for L12 and L13 (the ligands bearing the carboxylic group) with respect to L14 and L15 (bearing the phenolic unit) and L2 and L3 (bearing the vanillin units), due to the different net negative charge on the molecule (-3 for L12 and L13, and -2 for the remaining ligands). A similar behavior is observed for the second protonation constant on KA. Noticeable differences are also found between L12 and L13 depending on the different capabilities of forming stabilizing hydrogen bonds.

View Article Online
DOI: 10.1039/C7NJ03947F

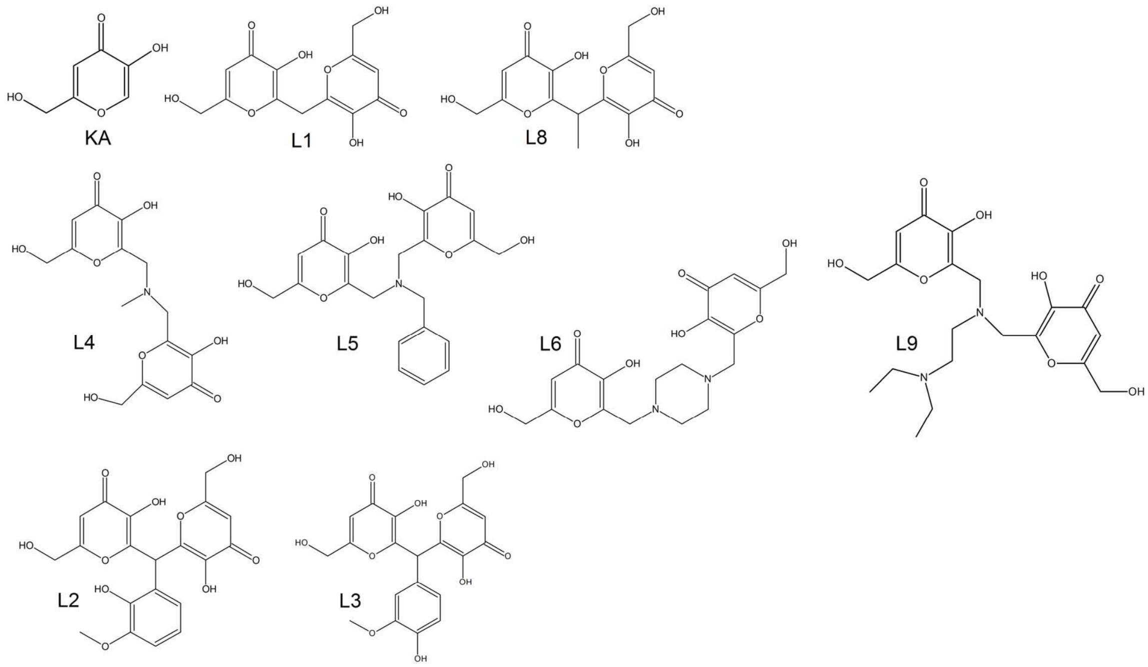

Scheme 4. Previously studied KA derivatives[22].

While the pFe and pAl values of L12-L15 are comparable to that of the similar ligand L2, the behavior of L3, characterized by extremely high pFe and pAl values, is difficult to explain. It is noteworthy that the highest pFe and pAl values are obtained by the L14 and L15 ligands, mainly related to their lower protonation constants. The ratios pM/pFe reported in Table 11 for all the KA derivatives studied by our group, even if highly scattered, reveal some trends. In particular, for the ligands with the shorter linker (apart L1, characterized by an extremely high pFe) the pAl/pFe ratios are the highest, and this depends on the

Table 11. Ratios pM/pFe for the L12-L15 ligands, and for other KA derivatives previously studied.

	KA	**L1**	**L8**	**L4**	**L5**	**L6**	**L9**	**L2**	**L3**	**L12**	**L13**	**L14**	**L15**
pAl/pFe	0.68	0.55	0.72	0.62	0.60	0.67	0.58	0.63	0.63	0.72	0.66	0.68	0.71
pCu/pFe	0.55	0.41	0.44	0.57	0.52	0.48	0.43	0.54	0.47	0.65	0.53	0.52	0.58
pZn/pFe	0.46	0.29	0.34	0.49	0.37	0.44	0.43	0.40	0.36	0.42	0.36	0.40	0.34

View Article Online

DOI: 10.1039/C7NJ03947F

smaller ionic radius of Al^{3+} compared to that of Fe^{3+}. No particular observation on copper and zinc ions can be made. At any rate, the pCu/pFe ratio in the range 0.4-0.6 and the pZn/pFe ratio in the range 0.3-0.5 imply a difference of about 9 and 11 units in the pM of copper and zinc ions respectively, and that of iron. This surely should prevent the interference of the essential Cu^{2+} and Zn^{2+} metal ions on iron chelation. On the other hand, the use of an excess of chelating agents than the amount necessary for iron chelation, and which is usually used in clinical treatments, can lead to the depletion of essential metal ions on the basis of the measured pCu and pZn values[15, 38, 39].

Conflicts of interest

There are no conflicts of interest to declare.

Acknowledgements

VMN, MAZ and MR acknowledge the financial support by MIUR-PRIN 2015 - 2015MP34H3_002. VMN thanks Fondazione Banco di Sardegna and Regione Autonoma della Sardegna, (Progetti Biennali di Ateneo Annualità 2016).

References

View Article Online
DOI: 10.1039/C7NJ03947F

1. G. Crisponi and M. Remelli, *Coordination Chemistry Reviews*, 2008, **252**, 1225-1240.

2. M. A. Santos, S. M. Marques and S. Chaves, *Coordination Chemistry Reviews*, 2012, **256**, 240-259.

3. G. Crisponi, V. M. Nurchi and M. A. Zoroddu, *Thalassemia Reports*, 2014, **4**, 13-18.

4. V. M. Nurchi, G. Crisponi, J. I. Lachowicz, S. Medici, M. Peana and M. A. Zoroddu, *Journal of Trace Elements in Medicine and Biology*, 2016, **38**, 10-18.

5. G. Crisponi, V. M Nurchi, M. Crespo-Alonso and L. Toso, *Current Medicinal Chemistry*, 2012, **19**, 2794-2815.

6. V. M. Nurchi, G. Crisponi, J. I. Lachowicz, S. Murgia, T. Pivetta, M. Remelli, A. Rescigno, J. Niclós-Gutíerrez, J. M. González-Pérez and A. Domínguez-Martín, *Journal of Inorganic Biochemistry*, 2010, **104**, 560-569.

7. V. M. Nurchi, J. I. Lachowicz, G. Crisponi, S. Murgia, M. Arca, A. Pintus, P. Gans, J. Niclos-Gutierrez, A. Domínguez-Martín, A. Castineiras, M. Remelli, Z. Szewczuk and T. Lis, *Dalton Transactions*, 2011, **40**, 5984-5998.

8. L. Toso, G. Crisponi, V. M. Nurchi, M. Crespo-Alonso, J. I. Lachowicz, M. A. Santos, S. M. Marques, J. Niclós-Gutiérrez, J. M. González-Pérez, A. Domínguez-Martín, D. Choquesillo-Lazarte and Z. Szewczuk, *Journal of Inorganic Biochemistry*, 2013, **127**, 220-231.

9. L. Toso, G. Crisponi, V. M. Nurchi, M. Crespo-Alonso, J. I. Lachowicz, D. Mansoori, M. Arca, M. A. Santos, S. M. Marques, L. Gano, J. Niclós-Gutíerrez, J. M. González-Pérez, A. Domínguez-Martín, D. Choquesillo-Lazarte and Z. Szewczuk, *Journal of Inorganic Biochemistry*, 2014, **130**, 112-121.

10. V. M. Nurchi, G. Crisponi, M. Arca, M. Crespo-Alonso, J. I. Lachowicz, M. A. Zoroddu, M. Peana, G. Pichiri, M. A. Santos, S. M. Marques, J. Niclos-Gutierrez, M. J. Gonzalez-Perez, A. Dominguez-Martin, D. Choquesillo-Lazarte, Z. Szewczuk, D. Mansoori and L. Toso, *Journal of Inorganic Biochemistry*, 2014, **141**, 132-143.

11. W. R. Harris, K. N. Raymond and F. L. Weitl, *Journal of the American Chemical Society*, 1981, **103**, 2667-2675.

View Article Online
DOI: 10.1039/C7NJ03947F

12. P. H. Fries, D. Imbert and A. Melchior, *The Journal of Chemical Physics*, 2010, **132**, 044502.

13. A. Melchior, E. Peralta, M. Valiente, C. Tavagnacco, F. Endrizzi and M. Tolazzi, *Dalton Transactions*, 2013, **42**, 6074-6082.

14. F. Endrizzi, A. Melchior, M. Tolazzi and L. Rao, *Dalton Transactions*, 2015, **44**, 13835-13844.

15. G. Crisponi, V. M. Nurchi, M. Crespo-Alonso, G. Sanna, M. A. Zoroddu, G. Alberti and R. Biesuz, *PLoS ONE*, 2015, **10**, e0133050.

16. A. Albert and E. P. Serjeant, *Ionization constants of acids and bases: a laboratory manual*, Methuen, 1962.

17. M. C. Aragoni, M. Arca, G. Crisponi, F. Cristiani, F. Isaia and V. M. Nurchi, *Talanta*, 1996, **43**, 1357-1366.

18. H. Irving, M. Miles and L. Pettit, *Analytica Chimica Acta*, 1967, **38**, 475-488.

19. G. Gran, *Analyst*, 1952, **77**, 661-671.

20. P. Gans, A. Sabatini and A. Vacca, *Talanta*, 1996, **43**, 1739-1753.

21. www.hyperquad.co.uk/HypSpec2014.htm.

22. V. M. Nurchi, T. Pivetta, J. I. Lachowicz and G. Crisponi, *Journal of Inorganic Biochemistry*, 2009, **103**, 227-236.

23. M. A. Zoroddu, M. Peana and S. Medici, *Dalton Transactions*, 2007, 379-384.

24. J. Lachowicz, V. Nurchi, G. Crisponi, M. Jaraquemada-Pelaez, M. Arca, A. Pintus, M. Santos, C. Quintanova, L. Gano and Z. Szewczuk, *Dalton Transactions*, 2016, **45**, 6517-6528.

25. M. Peana, S. Medici, V. M. Nurchi, J. I. Lachowicz, G. Crisponi, M. Crespo-Alonso, M. A. Santos and M. A. Zoroddu, *Journal of Inorganic Biochemistry*, 2015, **148**, 69-77.

View Article Online
DOI: 10.1039/C7NJ03947F

26. M. A. Zoroddu, S. Medici, M. Peana and R. Anedda, *Dalton Transactions*, 2010, **39**, 1282-1294.

27. S. Medici, M. Peana, L. G. Delogu and M. A. Zoroddu, *Dalton Transactions*, 2012, **41**, 4378-4388.

28. M. Remelli, M. Peana, S. Medici, L. G. Delogu and M. A. Zoroddu, *Dalton Transactions*, 2013, **42**, 5964-5974.

29. M. F. Peana, S. Medici, A. Ledda, V. M. Nurchi and M. A. Zoroddu, *The Scientific World Journal*, 2014, **2014**.

30. L. D. Hansen, T. E. Jensen, S. Mayne, D. J. Eatough, R. M. Izatt and J. J. Christensen, *The Journal of Chemical Thermodynamics*, 1975, **7**, 919-926.

31. P. Gans, A. Sabatini and A. Vacca, *Journal of Solution Chemistry*, 2008, **37**, 467-476.

32. A. Vacca, A. Sabatini and L. Bologni, *Dalton Transactions*, 1981, 1246-1250.

33. Bruker, *ESI Compass 1.3; DataAnalysis Version 4.0 (Build 234) Daltonik GmbH http://www.bdal.com*, .

34. G. Crisponi, M. Casu, V. M. Nurchi, F. Cesare-Marincola, T. Pivetta and R. Silvagni, *Talanta*, 2002, 56, 441-449.

35. G. R. Choppin, P. A. Bertrand, Y. Hasegawa and E. N. Rizkalla, *Inorganic Chemistry*, 1982, 21, 3722-3724.

36. M. C. Aragoni, M. Arca, G. Crisponi and V. M. Nurchi, *Analytica Chimica Acta*, 1995, 316, 195-204.

37. http://www.hyperquad.co.uk/HQ2013.htm, 2016.

38. J. I. Lachowicz, V. M. Nurchi, G. Crisponi, M. d. G. J. Pelaez, A. Rescigno, P. Stefanowicz, M. Cal and Z. Szewczuk, *Journal of Inorganic Biochemistry*, 2015, **151**, 36-43.

39. J. I. Lachowicz, V. M. Nurchi, G. Crisponi, M. G. Jaraquemada-Pelaez, M. Ostrowska, J. Jezierska, El. Gumienna–Kontecka, M. Peana, M. A. Zoroddu, D. Choquesillo-Lazarte, J. Niclós-Gutiérrez and J. M. González-Pérez, *J. Inorg. Biochem.*, 2015, **151,** 94-106.

View Article Online
DOI: 10.1039/C7NJ03947F

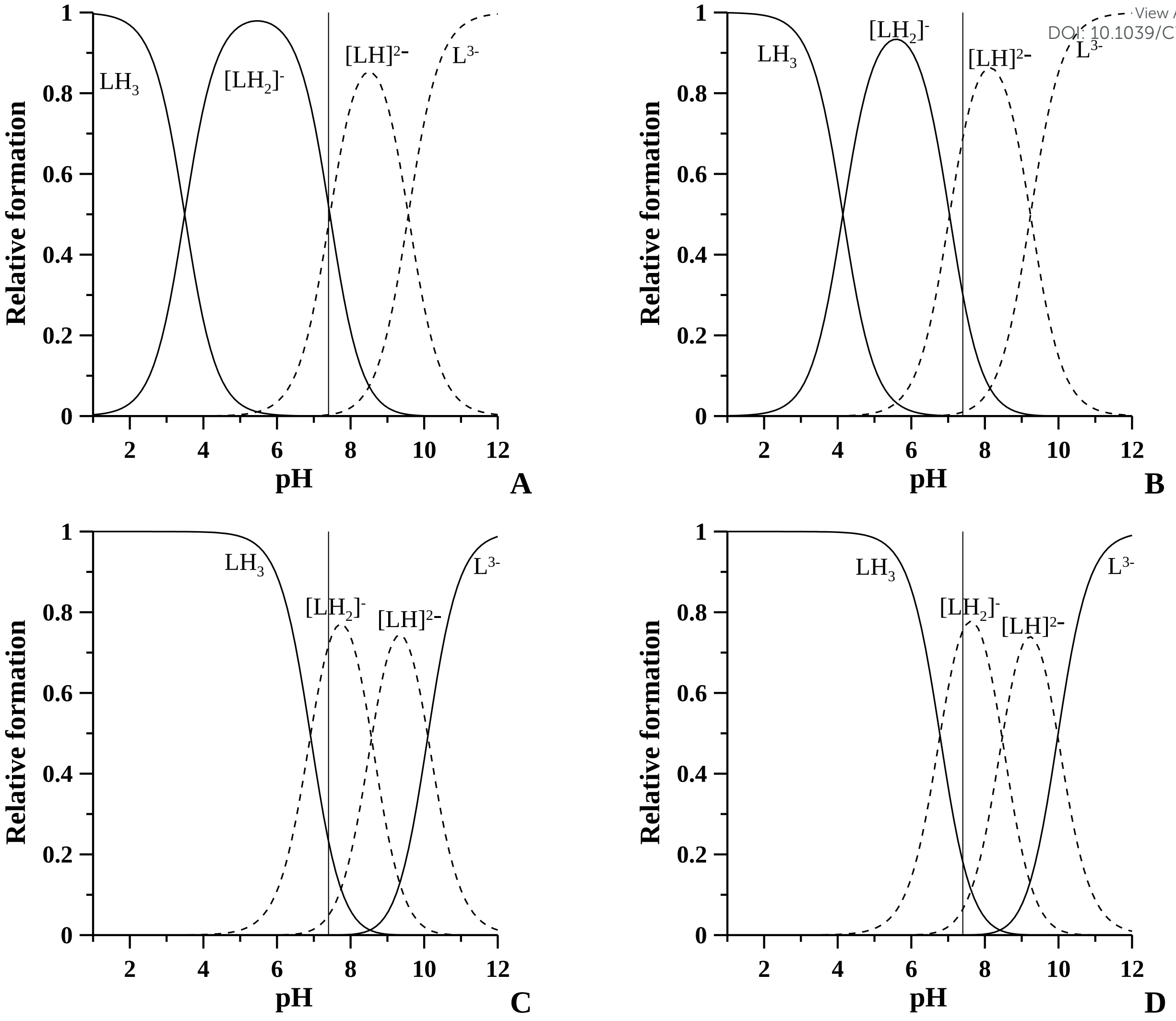

View Article Online
DOI: 10.1039/C7NJ03947F

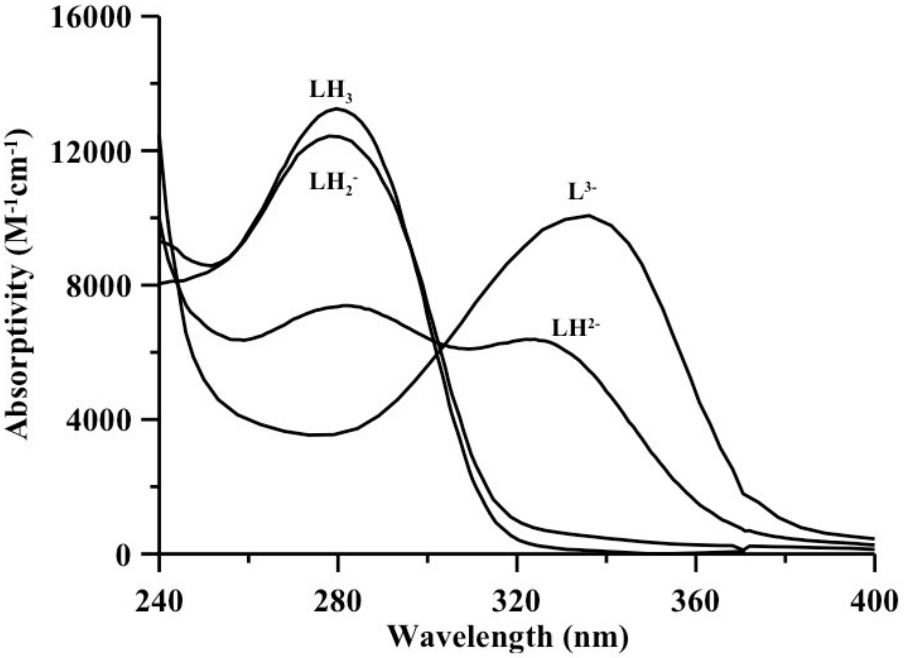

View Article Online
DOI: 10.1039/C7NJ03947F

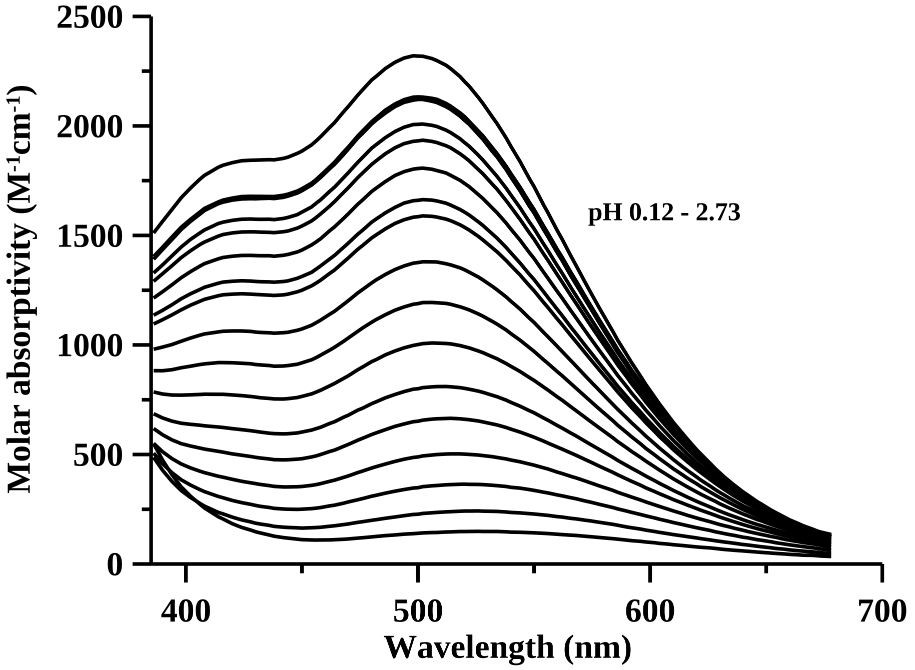

View Article Online
DOI: 10.1039/C7NJ03947F

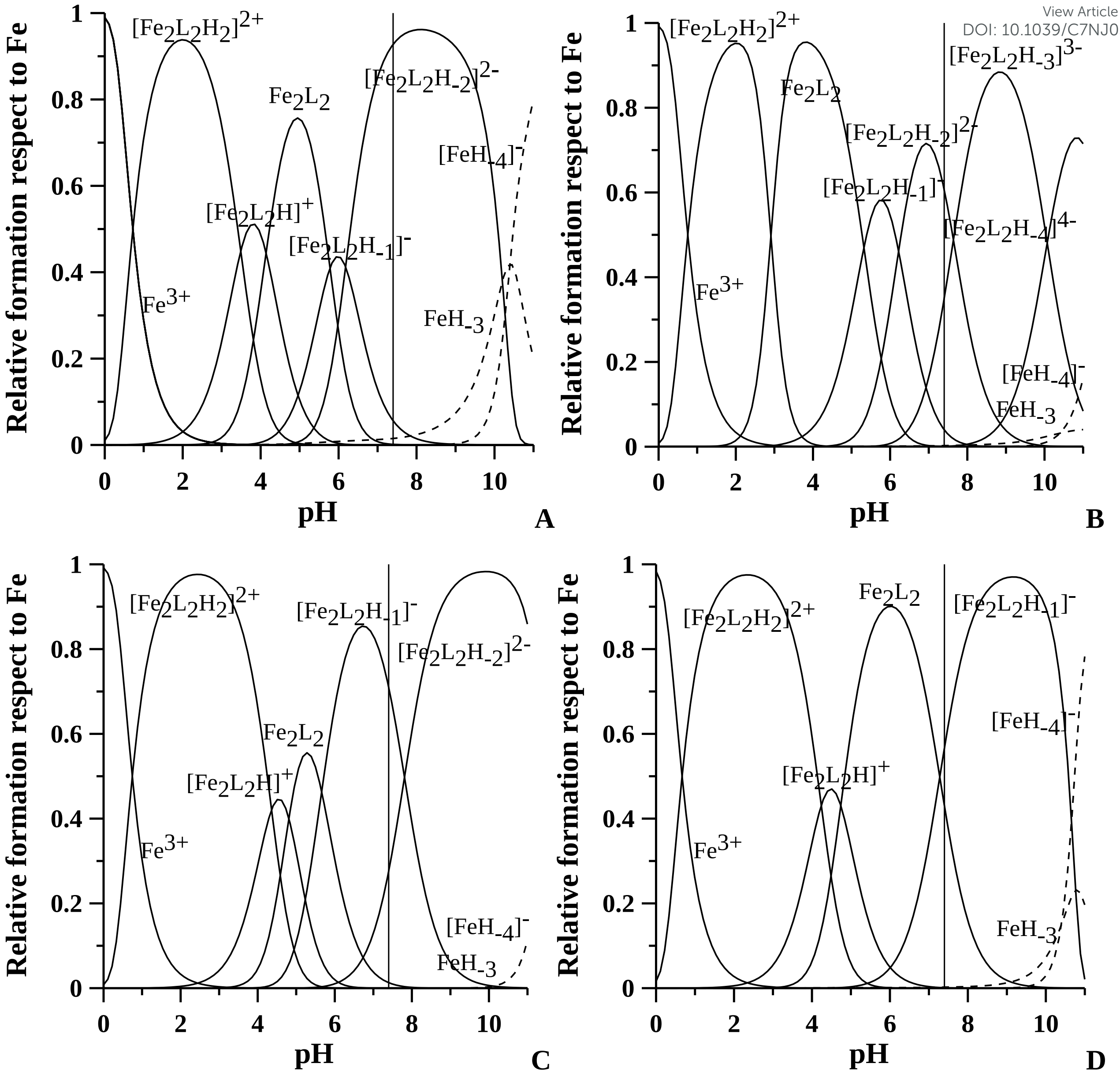

View Article Online
DOI: 10.1039/C7NJ03947F

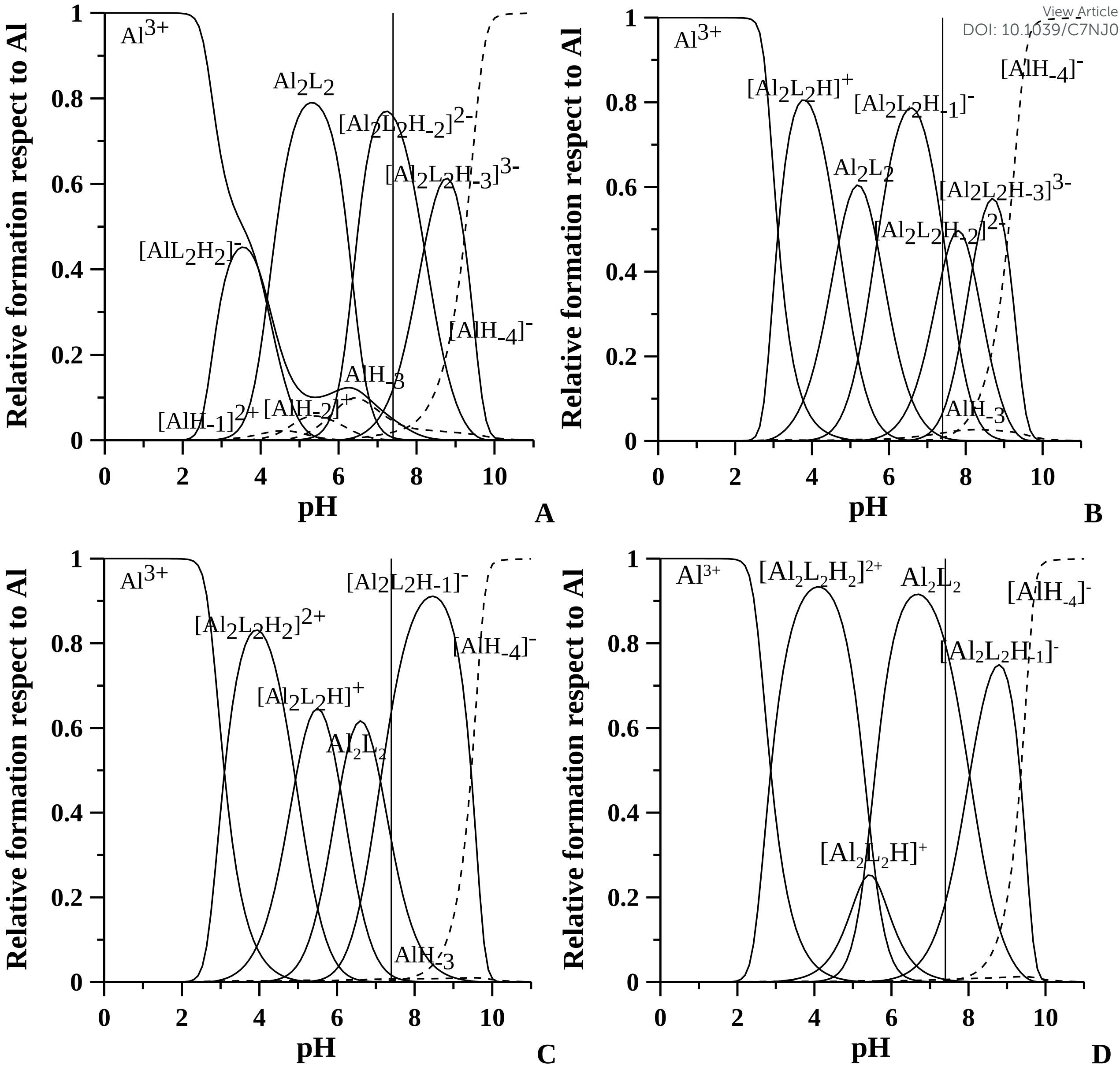

View Article Online
DOI: 10.1039/C7NJ03947F

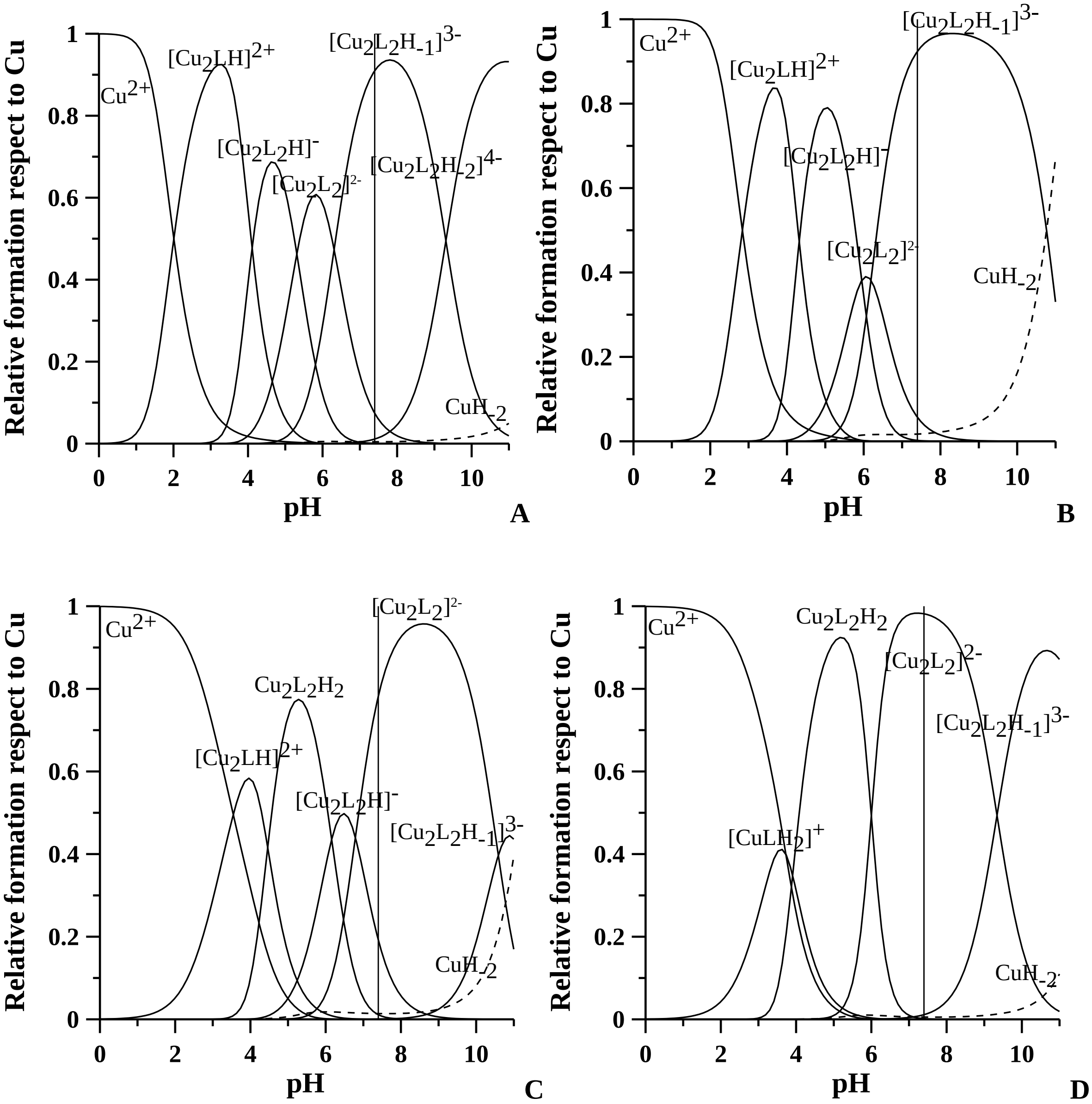

View Article Online
DOI: 10.1039/C7NJ03947F

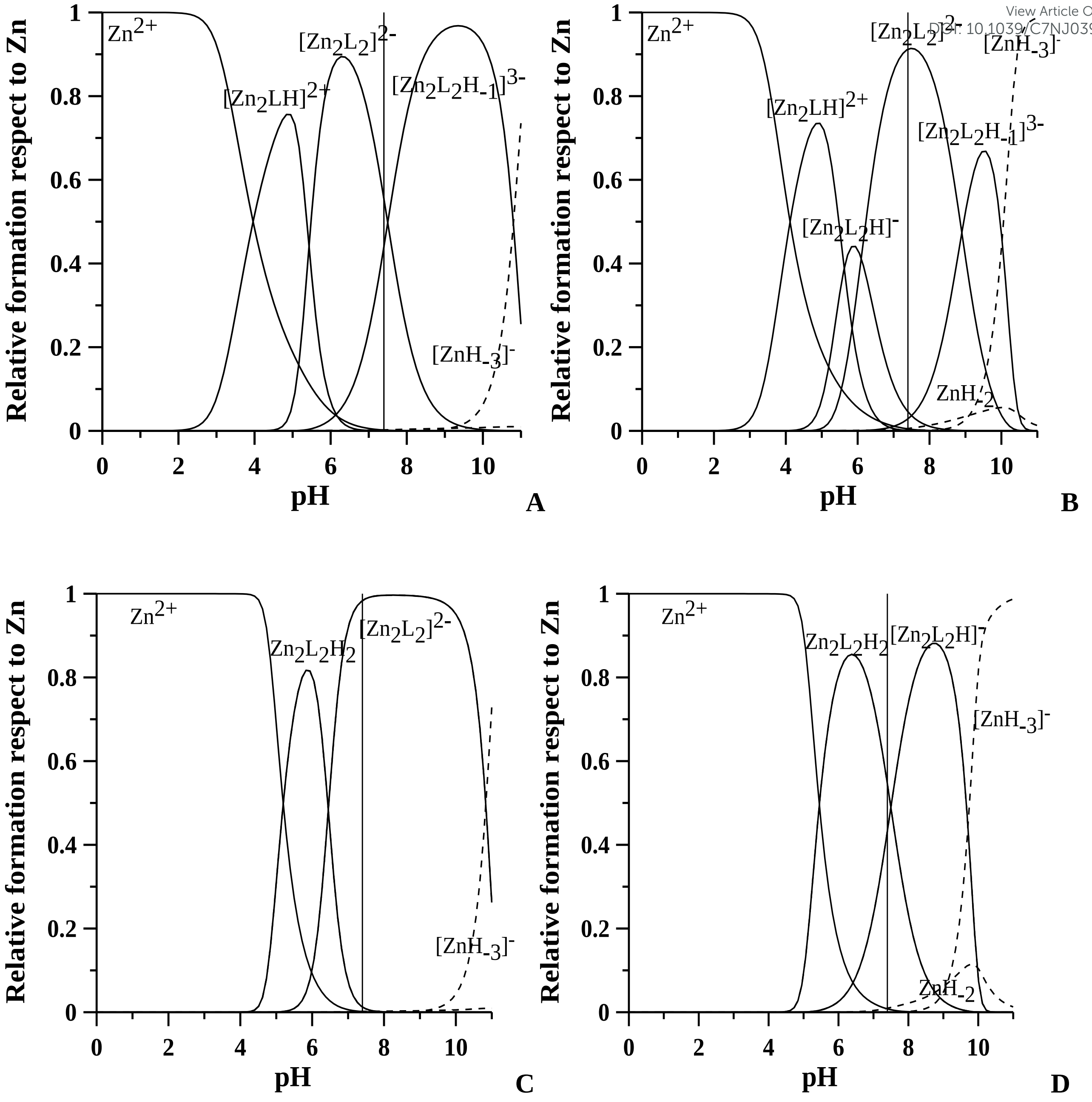

View Article Online
DOI: 10.1039/C7NJ03947F

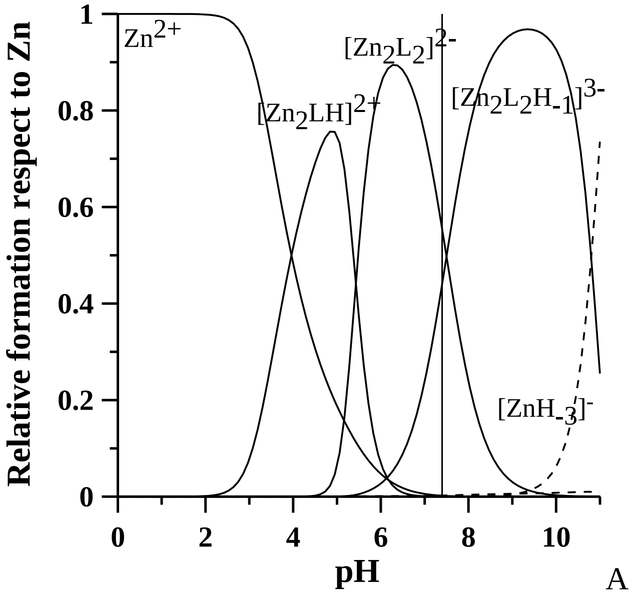

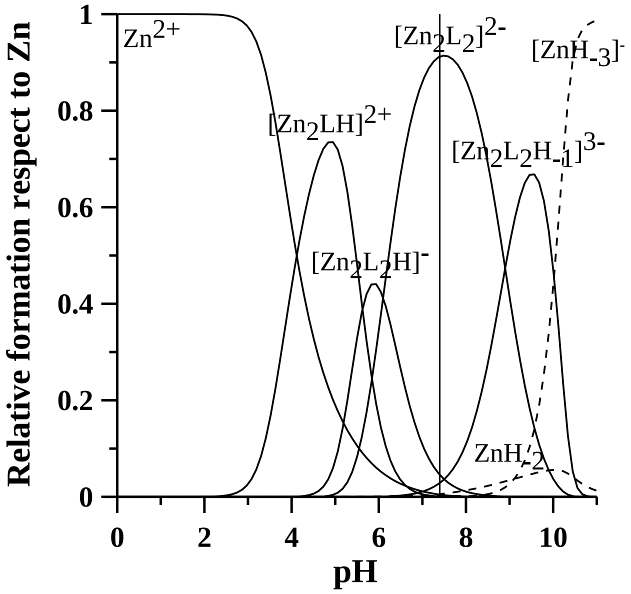

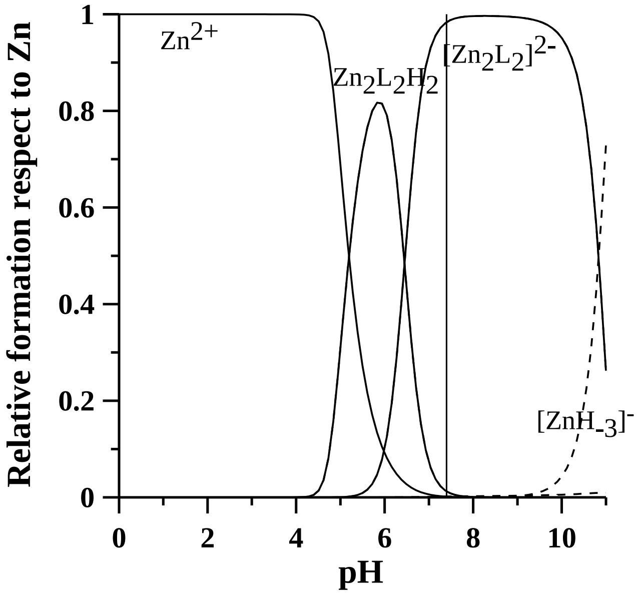

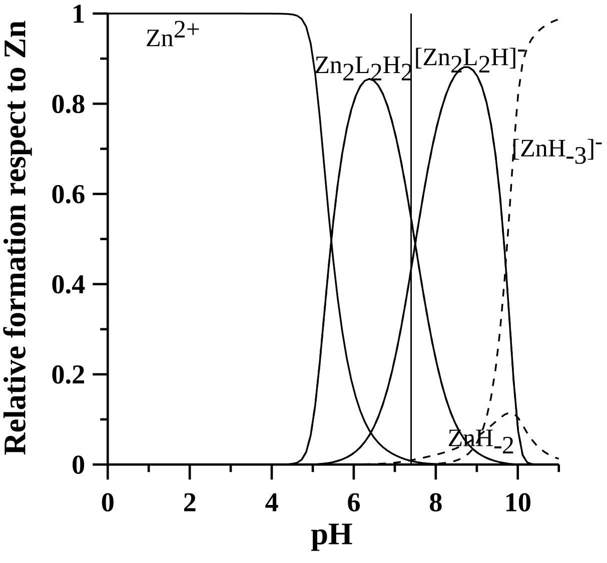

View Article Online
DOI: 10.1039/C7NJ03947F

Highlights

Four kojic acid derivatives were synthesized, and their chelation properties toward Fe^{3+}, Al^{3+}, Cu^{2+}, Zn^{2+} metal ions evaluated and discussed.

Graphical abstract